Hindawi Publishing Corporation
EURASIP Journal on Wireless Communications and Networking
Volume 2010, Article ID 256370, 9 pages
doi:10.1155/2010/256370

Research Article

A Semianalytical PDF of Downlink SINR for Femtocell Networks

Ki Won Sung,[1] Harald Haas,[2] and Stephen McLaughlin (EURASIP Member)[2]

[1] *KTH Royal Institute of Technology, 164 40 Kista, Sweden*
[2] *Institute for Digital Communications, The University of Edinburgh, King's Buildings, Edinburgh EH9 3JL, UK*

Correspondence should be addressed to Ki Won Sung, sungkw@kth.se

Received 31 August 2009; Revised 4 January 2010; Accepted 17 February 2010

Academic Editor: Ozgur Oyman

This paper presents a derivation of the probability density function (PDF) of the signal-to-interference and noise ratio (SINR) for the downlink of a cell in multicellular networks. The mathematical model considers uncoordinated locations and transmission powers of base stations (BSs) which reflect accurately the deployment of randomly located femtocells in an indoor environment. The derivation is semianalytical, in that the PDF is obtained by analysis and can be easily calculated by employing standard numerical methods. Thus, it obviates the need for time-consuming simulation efforts. The derivation of the PDF takes into account practical propagation models including shadow fading. The effect of background noise is also considered. Numerical experiments are performed assuming various environments and deployment scenarios to examine the performance of femtocell networks. The results are compared with Monte Carlo simulations for verification purposes and show good agreement.

1. Introduction

Signal-to-interference and noise ratio (SINR) is one of the most important performance measures in cellular systems. Its probability distribution plays an important role for system performance evaluation, radio resource management, and radio network planning. With an accurate probability density function (PDF) of SINR, the capacity and coverage of a system can be easily predicted, which otherwise should rely on complicated and time-consuming simulations.

There have been various approaches to investigate the statistical characteristics of received signal and interference. The other-cell interference statistics for the uplink of code division multiple access (CDMA) system was investigated in [1], where the ratio of other-cell to own-cell interference was presented. The result was extended to both the uplink and the downlink of general cellular systems by [2]. In [3], the second-order statistics of SIR for a mobile station (MS) were investigated. In [4, 5], the prediction of coverage probability was addressed which is imperative in the radio network planning process. The probability that SINR goes below a certain threshold, which is termed outage probability, is another performance measure that has been extensively explored. The derivation of the outage probability can be found in [6–8] and references therein.

While most of the contributions have focused on a particular performance measure such as coverage probability or outage probability, an explicit derivation of the probability distribution for signal and interference has also been investigated [9, 10]. In [9], a PDF of adjacent channel interference (ACI) was derived in the uplink of cellular system. A PDF of SIR in an ad hoc system was studied in [10] assuming single transmitter and receiver pair.

In this paper, we derive the PDF of the SINR for the downlink of a cell area in a semianalytical fashion. A practical propagation loss model combined with shadow fading is considered in the derivation of the PDF. We also consider background noise in the derivation, which is often ignored in the references. Uncoordinated locations and transmission powers of interfering base stations (BSs) are considered in the model to take into account the deployment of femtocells (or home BSs) [11] in an indoor environment. It has been suggested that femto BSs can significantly improve system spectral efficiency by up to a factor of five [12]. It has also been found that in closed-access femtocell networks macrocell MSs in close vicinity to a femtocell greatly suffer from high interference and that such macrocell MSs cause destructive interference to femtocell BSs [13]. Thus, an accurate model for the probability distribution of the SINR

assuming an uncoordinated placement of indoor BSs can be vital for further system improvements. In spite of the recent efforts for the performance evaluation of femtocells, most of the works relied on system simulation experiments [12–17]. To the best of our knowledge, the PDF of SINR for the outlined conditions and environment has not been derived before.

Since shadow fading is generally considered to follow a log-normal distribution, the PDF of the sum of log-normal RVs should be provided as a first step in the derivation of the SINR distribution. During the last few decades numerous approximations have been proposed to obtain the PDF of the sum of log-normal RVs since the exact closed-form expression is still unknown [18–23]. So far, no method offers significant advantages over another [18], and sometimes a tradeoff exists between the accuracy of the approximation and the computational complexity. We adopt two methods of approximation proposed by Fenton and Wilkinson [19] and Mehta et al. [20] which provide a good balance between accuracy and complexity. The performance of both methods is examined in various environments and a guideline is provided for choosing one of the methods.

The derivation of SINR distribution in this paper is semi-analytical in the sense that the PDF can be easily calculated by applying standard numerical methods to equations obtained from analysis. Numerical experiments are performed to investigate the effects of standard deviation of shadow fading, the number of interfering BSs, wall penetration loss, and transmission powers of BSs. The results obtained are also validated by comparison with Monte Carlo simulations.

The paper is organised as follows. In Section 2, the PDF of the downlink SINR is derived. Numerical experiments are performed in various environments and the results are compared with Monte Carlo simulations in Section 3. Finally, the conclusions are provided in Section 4.

2. Derivation of the PDF of Downlink SINR

The derivation of the PDF of downlink SINR is divided into two parts. First, the SINR of an arbitrary MS is expressed depending on its location in Section 2.1. Methods of approximating the sum probability distribution of log-normal RVs are discussed and adopted in the SINR derivation. Second, the PDF of SINR unconditional on the location of the MS is derived in Section 2.2.

2.1. Location-Dependent SINR. Let us consider a femtocell which will be termed the cell of interest (CoI). The CoI is assumed to be circular with a cell radius R. We assume the MSs in the CoI to be uniformly distributed in the cell area. An arbitrary MS m is considered whose location is (r_m, θ_m), where $0 \le r_m \le R$ and $0 \le \theta_m \le 2\pi$. The MS m receives interference from L BSs that are a mixture of femto and macro-BSs. The network is modelled using polar coordinates where the BS of the CoI is located at the center and the location of the jth interfering BS is denoted by $(r_b(j), \theta_b(j))$. In a practical deployment of femtocell systems, the placement of BSs in a random and uncoordinated fashion is unavoidable and may generate high interference scenarios and dead spots particularly in an indoor environment.

Let P_s^t be the transmission power of the BS in the CoI. It is attenuated by path loss and shadow fading. Let X_s be the RV which models the shadow fading. It is generally assumed that X_s follows a Gaussian distribution with zero mean and variance $\sigma_{X_s}^2$ in dB. Thus the received signal power at the MS m from the serving BS, P_s^r, is denoted by

$$P_s^r = P_s^t G_b G_m C_s {r_m}^{-\alpha_s} \exp(\beta X_s), \tag{1}$$

where G_b and G_m are antenna gains of the BS and the MS, respectively, C_s is constant of path loss in the CoI, α_s is path loss exponent of CoI, and $\beta = \ln(10)/10$. The $\ln(\cdot)$ denotes natural logarithm. P_s^r can be rewritten as follows:

$$P_s^r = \exp[\ln(P_s^t G_b G_m C_s) - \alpha_s \ln r_m + \beta X_s]. \tag{2}$$

Note that an RV $Y = \exp(V)$ follows a log-normal distribution if V is a Gaussian distributed RV. Thus, P_s^r follows a log-normal distribution conditioned on the location of MS m. The PDF of P_s^r is given by

$$f_{P_s^r}(z \mid r_m, \theta_m) = \frac{1}{z\sigma_s\sqrt{2\pi}} \exp\left[\frac{-(\ln z - \mu_s)^2}{2\sigma_s^2}\right], \tag{3}$$

where $\mu_s = \ln(P_s^t G_b G_m C_s) - \alpha_s \ln r_m$ and $\sigma_s^2 = \beta^2 \sigma_{X_s}^2$.

Let I_j^r be the received interference power from the jth interfering BS. By denoting P_j^t as the transmission power from the jth BS, I_j^r results in

$$I_j^r = P_j^t G_b G_m C_j d_{mb}(j)^{-\alpha_j} \exp\left(\beta X_j\right), \tag{4}$$

where C_j and α_j are the path loss constant and exponent, respectively, on the link between the jth BS and MS m, and X_j is a Gaussian RV for shadow fading with zero mean and variance $\sigma_{X_j}^2$ on the link between the jth BS and MS m. Note that the transmission power of each interfering BS can be different since an uncoordinated femtocell deployment is considered. Path loss parameters and standard deviation of shadow fading can also be different in each BS in practical systems. The distance between MS m and the jth interfering BS is $d_{mb}(j)$, which is obtained from

$$d_{mb}(j) = \left[r_m^2 + r_b(j)^2 - 2 r_m r_b(j) \cos(\theta_m - \theta_b(j))\right]^{1/2}. \tag{5}$$

In a similar fashion to P_s^r, I_j^r follows a log-normal distribution with PDF given by

$$f_{I_j^r}(z \mid r_m, \theta_m) = \frac{1}{z\sigma_j\sqrt{2\pi}} \exp\left[\frac{-\left(\ln z - \mu_j\right)^2}{2\sigma_j^2}\right], \tag{6}$$

where $\mu_j = \ln(P_j^t G_b G_m C_j) - \alpha_j \ln d_{mb}(j)$ and $\sigma_j^2 = \beta^2 \sigma_{X_j}^2$.

Background noise can be regarded as a constant value by assuming the constant noise figure and the noise temperature. Let N_{bg} be the background noise power at MS m, given by

$$N_{bg} = kTW\varphi, \tag{7}$$

where k is the Boltzmann constant, T is the ambient temperature in Kelvin, W is the channel bandwidth, and φ is the noise figure of the MS. In order to make N_{bg} mathematically tractable, we introduce an auxiliary Gaussian RV X_n with *zero* mean and *zero* variance so that N_{bg} can be treated as log-normal RV with parameters of $\mu_n = \ln(kTW\varphi)$ and $\sigma_n = 0$. Note that N_{bg} has a constant value, and this is accounted for by the fact that the defined RV has zero variance. This particular definition is useful for the determination of the final PDF. By introducing X_n, N_{bg} can be rewritten as follows:

$$N_{bg} = kTW\varphi \exp(X_n) = \exp[\ln(kTW\varphi) + X_n]. \quad (8)$$

Let us consider a system with no interference arising from the serving cell such as an OFDMA or a TDMA system. The downlink SINR of MS m is denoted by γ_m, which is given by

$$\gamma_m = \frac{P_s^r}{\sum_{j=1}^{L} I_j^r + N_{bg}} = \frac{P_s^r}{\Upsilon}. \quad (9)$$

In (9), Υ denotes the sum of the interference powers and the background noise power. Since all of I_j^r and N_{bg} are log-normally distributed, Υ is the sum of $L + 1$ log-normal RVs. Note that the exact closed-form expression is not known for the PDF of the sum of log-normal RVs. The most widely accepted approximation approach is to assume that the sum of log-normal RVs follows a log-normal distribution. Various methods have been proposed to find out parameters of the distribution [19–21].

Let $Y_1, \ldots, Y_M$ be M independent but not necessarily identical log-normal RVs, where $Y_j = \exp(V_j)$ and V_j is a Gaussian distributed RV with mean μ_{V_j} and variance $\sigma_{V_j}^2$. The sum of M RVs is denoted by Y such that $Y = \sum_{j=1}^{M} Y_j$. Approximations assume that Y follows a log-normal distribution with parameters μ_V and σ_V^2.

The Fenton and Wilkinson (FW) method [19] is one of the most frequently adopted approximations in literature. It obtains μ_V and σ_V^2 by assuming that the first and second moments of Y match the sum of the moments of Y_j. It should be noted that the FW method is the only approximate method that provides a closed-form expression of μ_V and σ_V^2 [20]. Let us denote μ_n as μ_{L+1} and σ_n as σ_{L+1}. From [19], the PDF of Υ conditioned on the location of MS m is given as follows:

$$f_\Upsilon(z \mid r_m, \theta_m) = \frac{1}{z\sigma_\Upsilon\sqrt{2\pi}} \exp\left[\frac{-(\ln z - \mu_\Upsilon)^2}{2\sigma_\Upsilon^2}\right], \quad (10)$$

where μ_Υ and σ_Υ^2 are given by

$$\sigma_\Upsilon^2 = \ln\left[\frac{\sum_{j=1}^{L+1} \exp\left(2\mu_j + \sigma_j^2\right)\left(\exp\left(\sigma_j^2\right) - 1\right)}{\left[\sum_{j=1}^{L+1} \exp\left(\mu_j + \sigma_j^2/2\right)\right]^2} + 1\right],$$
$$\mu_\Upsilon = \ln\left[\sum_{j=1}^{L+1} \exp\left(\mu_j + \frac{\sigma_j^2}{2}\right)\right] - \frac{\sigma_\Upsilon^2}{2}. \quad (11)$$

In spite of its simplicity, the accuracy of the FW method suffers at high values of $\sigma_{V_j}^2$. This means that the method may break down when an MS experiences a large standard deviation of shadow fading from interfering BSs. Thus, we adopt another method of approximating the sum of log-normal RVs which gives a more accurate result at a cost of increased computational complexity.

The method proposed in [20], which is called MWMZ method in this paper after the initials of authors, exploits the property of the moment-generating function (MGF) that the product of MGFs of independent RVs equals to the MGF of the sum of RVs. The MGF of RV Y is defined as

$$\Psi_Y(s) = \int_0^\infty \exp(-sy) f_Y(y) dy. \quad (12)$$

By the property of MGF,

$$\Psi_Y(s) = \prod_{j=1}^{M} \Psi_{Y_j}(s). \quad (13)$$

While the closed-form expression for the MGF of log-normal distribution is not available, a series expansion based on Gauss-Hermite integration was employed in [20] to approximate the MGF. For a real coefficient s, the MGF of the log-normal RV Y is given by

$$\hat{\Psi}_Y(s; \mu_V, \sigma_V) \triangleq \sum_{j=1}^{M} \frac{w_j}{\sqrt{\pi}} \exp\left[-s \exp\left(\sqrt{2}\sigma_V a_j + \mu_V\right)\right], \quad (14)$$

where w_j and a_j are weights and abscissas of the Gauss-Hermite series which can be found in [24, Table 25.10]. From (13), a system of two nonlinear equations can be set up with two real and positive coefficients s_1 and s_2 as follows:

$$\sum_{j=1}^{M} \frac{w_j}{\sqrt{\pi}} \exp\left[-s_i \exp\left(\sqrt{2}\sigma_V a_j + \mu_V\right)\right] = \prod_{j=1}^{M} \hat{\Psi}_{Y_j}\left(s_i; \mu_{V_j}, \sigma_{V_j}\right), \quad i = 1, 2. \quad (15)$$

The variables to be solved by (15) are μ_V and σ_V. The right-hand side of (15) is a constant value which can be calculated with known parameters.

By employing (15), μ_Υ and σ_Υ^2 in (10) can be effectively obtained by standard numerical methods such as the function "fsolve" in Matlab. The coefficient $\mathbf{s} = (s_1, s_2)$ adjusts weight of penalty for inaccuracy of the PDF. Increasing $\mathbf{s}$ imposes more penalty for errors in the head portion of the PDF of Y, whereas smaller $\mathbf{s}$ penalises errors in the tail portion. Thus, smaller $\mathbf{s}$ is recommended if one is interested in the PDF of poor SINR region, while larger $\mathbf{s}$ should be used to examine statistics of higher SINR.

As shown in (3), the received signal power, P_s^r, follows a log-normal distribution. The sum of the received interference and the background noise power, Υ, was also approximated as a log-normal RV. Thus, the SINR of the MS m, γ_m, is the ratio of two log-normal RVs, which also follows

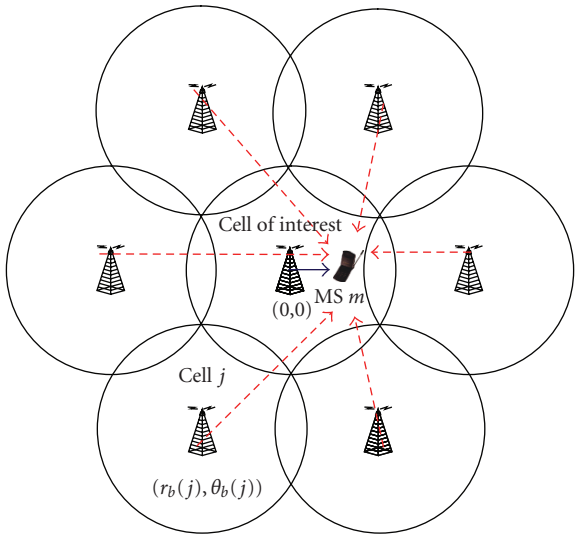

Figure 1: Locations of the CoI and the interfering BSs.

Table 1: Simulation parameters.

Parameter	Value
Cell radius	50 m
Path loss exponent	3.68
Path loss constant	43.8 dB
Center frequency	5.25 GHz
Channel bandwidth	10 MHz
MS noise figure	7 dB
BS transmission power	20 dBm
BS antenna gain	3 dBi
MS antenna gain	0 dBi
Number of interfering cells	6
Frequency reuse factor	1

Table 2: Kullback-Leibler Distance between the simulation and the analysis ($\times 10^{-4}$).

σ_{X_s} and σ_{X_j} [dB]	FW method	MWMZ method
3	6.00	6.98
4	3.66	4.34
5	11.32	6.05
6	35.70	8.81
7	90.50	12.29
8	186.87	16.24
9	324.10	21.23
10	489.04	26.13

a log-normal distribution. From (3) and (10), the PDF of γ_m is shown as

$$f_{\gamma_m}(z \mid r_m, \theta_m) = \frac{1}{z\sigma_{\gamma_m}\sqrt{2\pi}} \exp\left[\frac{-\left(\ln z - \mu_{\gamma_m}\right)^2}{2\sigma_{\gamma_m}^2}\right], \quad (16)$$

where $\mu_{\gamma_m} = \mu_s - \mu_Y$ and $\sigma_{\gamma_m}^2 = \sigma_s^2 + \sigma_Y^2$.

2.2. The PDF of Downlink SINR in a Cell. Up to this point, the PDF of the downlink SINR has been derived conditionally on the location of the MS m. Let us denote the location of MS m by ρ. Since it is assumed that MSs are uniformly distributed within a circular area, the PDF of ρ, $f_\rho(r_m, \theta_m)$, is as follows:

$$f_\rho(r_m, \theta_m) = \frac{r_m}{\pi R^2}. \quad (17)$$

From (16) and (17), the joint distribution of the SINR and the MS location is

$$f_{\gamma_m,\rho}(z, r_m, \theta_m) = f_{\gamma_m}(z \mid r_m, \theta_m) f_\rho(r_m, \theta_m) = \frac{r_m}{z\sigma_{\gamma_m} R^2 \sqrt{2\pi^3}} \exp\left[\frac{-\left(\ln z - \mu_{\gamma_m}\right)^2}{2\sigma_{\gamma_m}^2}\right]. \quad (18)$$

Let γ be the RV of the downlink SINR of an MS in an arbitrary location within a circular cell area. The PDF of γ can be obtained by integrating $f_{\gamma_m,\rho}(z, r_m, \theta_m)$ over r_m and θ_m. Thus, we get

$$f_\gamma(z) = \int_0^R \int_0^{2\pi} \frac{r_m}{z\sigma_{\gamma_m} R^2 \sqrt{2\pi^3}} \exp\left[\frac{-\left(\ln z - \mu_{\gamma_m}\right)^2}{2\sigma_{\gamma_m}^2}\right] d\theta_m dr_m. \quad (19)$$

Note that μ_{γ_m} in (19) is a function of (r_m, θ_m). We employ numerical integration methods to obtain the final PDF.

3. Numerical Results

The PDF of downlink SINR derived in (19) is calculated numerically and compared with a Monte Carlo simulation result in order to validate the analysis. We consider the nonline of sight (NLOS) indoor environment at 5.25 GHz as specified in [25, page 19] to be the basic environment for the comparison. The path loss formula is given as follows:

$$\mathrm{PL}(d) = 43.8 + 36.8 \log_{10}\left(\frac{d}{d_0}\right), \quad (20)$$

where d_0 is a reference distance in the far field. The interfering BSs are assumed to be femto BSs located on the same floor of a building throughout the experiments. However, interference scenarios such as femto BSs in different floors or outdoor macro-BSs can be easily examined by employing appropriate path loss models. The basic parameters used for the comparison are summarised in Table 1.

We assume that all interfering BSs are located at the same distance from the serving BS as shown in Figure 1. Cells are assumed to overlap each other to consider a dense deployment of the femto BSs. Although it is unlikely that the interfering BSs are in regular shapes in practical deployments, it is useful to consider this topology for examining the effects of parameters such as standard deviation of shadow fading, the number of BSs, wall penetration loss, and transmission power of BSs. It should be emphasised that the

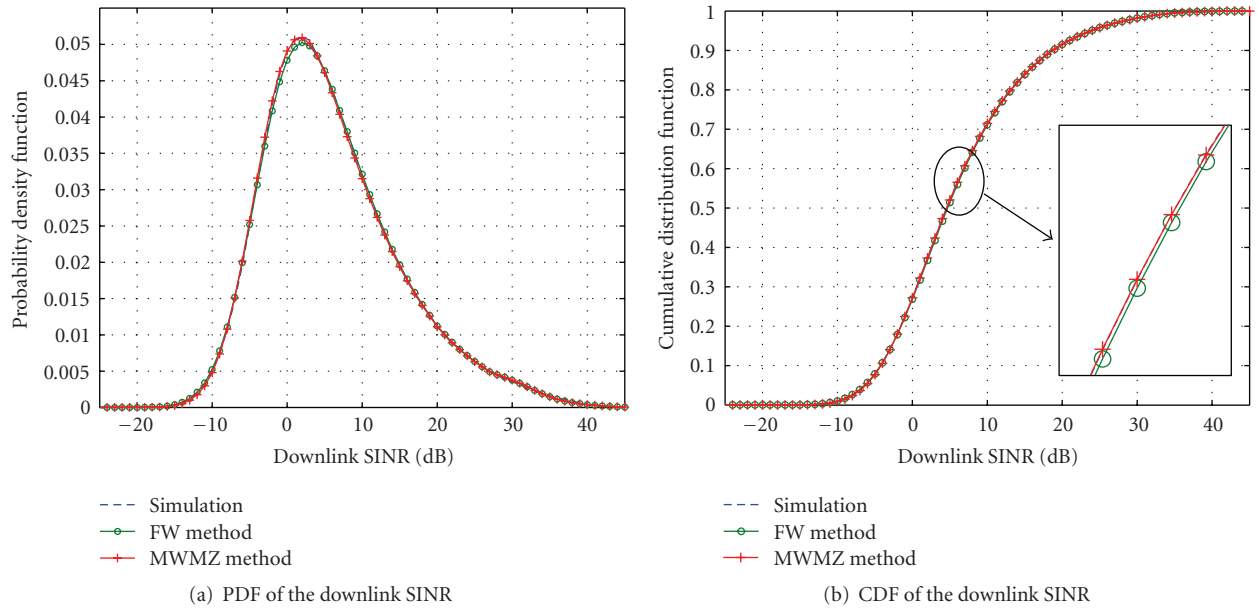

(a) PDF of the downlink SINR (b) CDF of the downlink SINR

Figure 2: A comparison of the PDF and CDF obtained by the analysis with the result of Monte Carlo simulation ($\sigma_{X_s} = \sigma_{X_j} = 3.5$ dB).

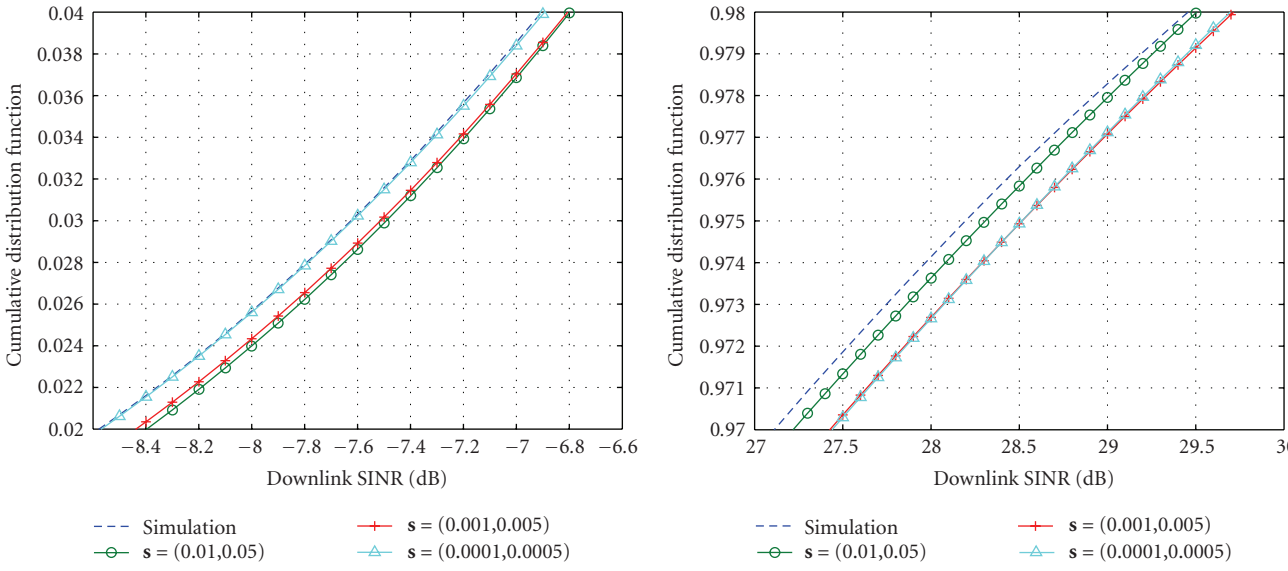

(a) Tail portion of the CDF (b) Head portion of the CDF

Figure 3: Impact of **s** on the performance of MWMZ method: tail and head portions of CDF ($\sigma_{X_s} = \sigma_{X_j} = 3.5$ dB).

PDF derived in Section 2 can effectively take into account irregular locations and transmission powers of BSs.

The result of the comparison is illustrated in Figure 2 where the PDFs derived by FW and MWMZ methods are compared with the Monte Carlo simulation result in Figure 2(a) and the cumulative distribution functions (CDFs) of the PDFs are depicted in Figure 2(b). The standard deviation of shadow fading, σ_{X_s} and σ_{X_j}, is considered to be 3.5 dB since it represents a typical value in an indoor office environment according to the measurement results in [25]. It is observed that the numerically obtained PDFs from both of the methods are in good agreement with the Monte Carlo simulation.

The impact of the parameter **s** on the performance of MWMZ method is shown in Figure 3 where the tail portion of the CDF (low SINR region) is depicted in Figure 3(a) and the head portion of the CDF (high SINR regime) is illustrated in Figure 3(b). Smaller **s** tends to give more accurate match in low SINR region while resulting in larger error in high SINR region. $\mathbf{s} = (0.01, 0.05)$ is chosen in the experiments since it brings about relatively small difference from simulations throughout the whole SINR region.

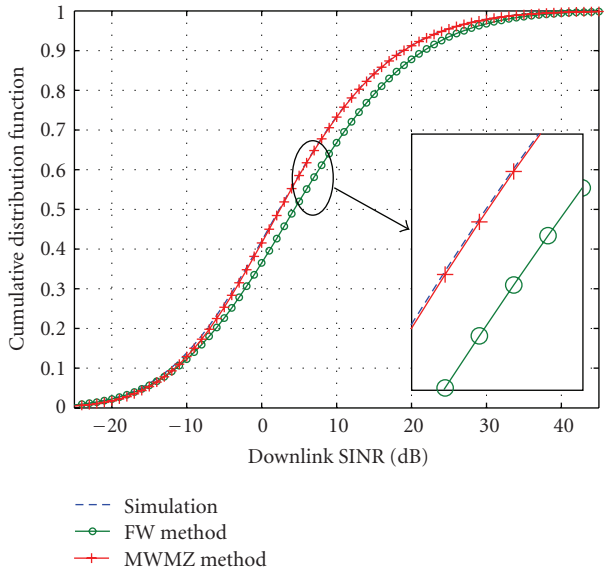

Figure 4: A comparison of the CDF obtained by the analysis with the result of Monte Carlo simulation ($\sigma_{X_s} = \sigma_{X_j} = 8.0$ dB).

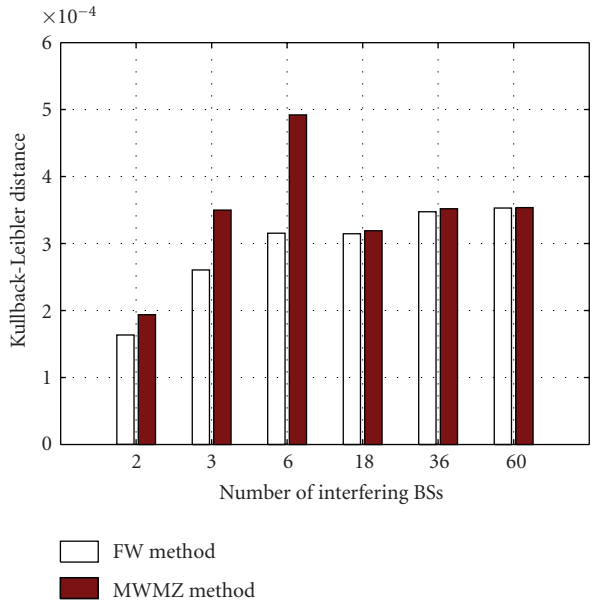

Figure 5: Kullback-Leibler Distance between simulation and analysis ($\sigma_{X_s} = \sigma_{X_j} = 3.5$ dB).

Figure 4 shows the CDFs when the standard deviation of shadow fading is 8.0 dB. While the SINR obtained by MWMZ method is still in good agreement with the simulation result, the difference between the analysis and the simulation is apparent in case of FW method. It means that FW method cannot be used in an environment where high shadow fading is experienced by MSs. In order to quantify the effect of shadow fading standard deviation, we introduce *Kullback-Leibler Distance* (KLD) which is a measure of divergence

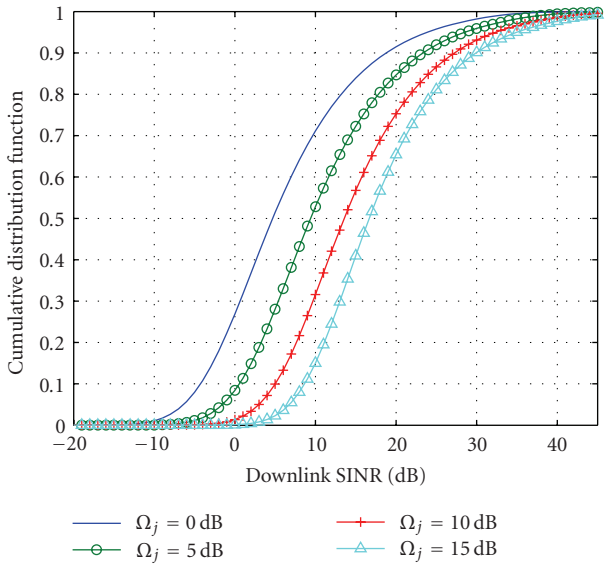

Figure 6: Effect of wall penetration loss on CDF of SINR (FW method, $\sigma_{X_s} = \sigma_{X_j} = 3.5$ dB).

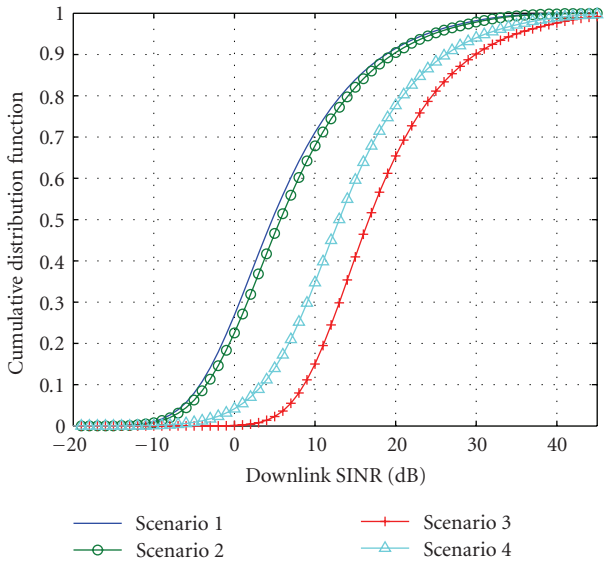

Figure 7: Effect of different wall penetration losses on CDF of SINR (FW method, $\sigma_{X_s} = \sigma_{X_j} = 3.5$ dB).

between two probability distributions [26]. For the two PDFs $p(x)$ and $q(x)$ the KLD is defined as

$$D(p\|q) = \int p(x)\log_2\frac{p(x)}{q(x)}dx. \tag{21}$$

The KLD is a nonnegative entity which measures the difference of the *estimated* distribution $q(x)$ from the *real* distribution $p(x)$ in a statistical sense. It becomes zero if and only if $p(x) = q(x)$. Table 2 presents the KLD for various standard deviations of shadow fading by assuming that the simulation results represent the true PDFs of SINR. It is shown in the table that the KLD of FW method soars when

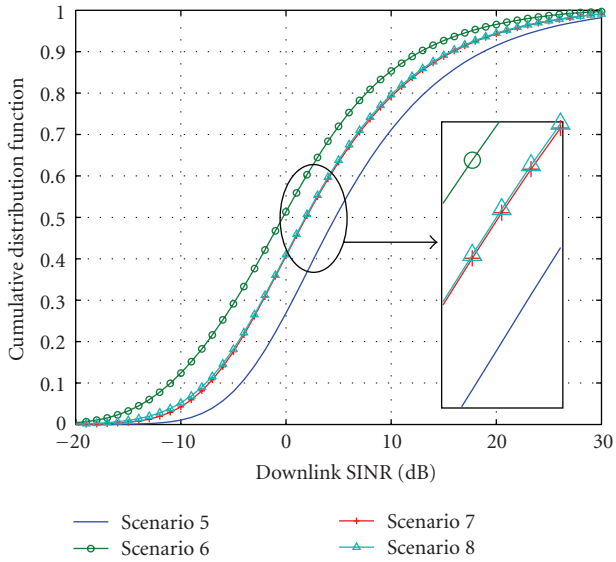

Figure 8: CDF of SINR with uncoordinated BS transmission power (FW method, $\sigma_{X_s} = \sigma_{X_j} = 3.5$ dB).

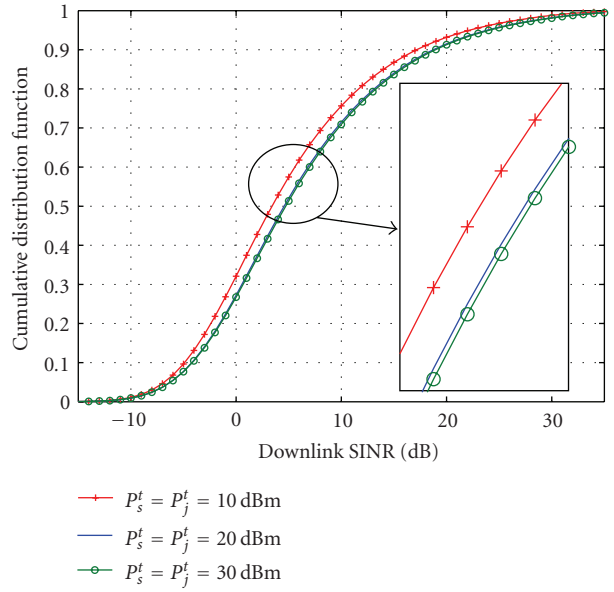

Figure 9: Effect of BS transmission power and background noise on CDF of SINR (FW method, $\sigma_{X_s} = \sigma_{X_j} = 3.5$ dB).

the standard deviation of shadow fading is higher than 6 dB. This implies that the range of standard deviation in which FW method can be adopted is between 3 dB and 6 dB, which is a typical range of shadow fading in an in-building environment [14, 25]. On the contrary, the MWMZ method maintains an acceptable level of the KLD even for the high shadow fading standard deviation. FW method is preferred if both of the methods are applicable due to its simplicity.

The effect of the number of interfering BSs is examined in Figure 5. It is known that the sum of log-normal RVs is not accurately approximated by a log-normal distribution as the number of summands increases [22]. This means that the derived SINR may not be accurate for a large number of interfering BSs. Figure 5 shows the KLD of FW and MWMZ methods compared to simulation results when L is between 2 and 60. An impairment in the accuracy is not observed as L increases, which means that the derivation of SINR in this paper is useful for the practical range of interfering BSs in the downlink of cellular systems.

The numerical results so far have focused on the verification of the derived PDF. Now we investigate the performance of femtocell network in various environments. An important observation in Figure 2 is that the probability of the SINR below 2.2 dB (a typical threshold for binary phase shift keying (BPSK) to achieve reasonable BER performance [27]) is about 0.38 for the parameters in Table 1. In other words, the outage probability is around 38%. This means that a dense deployment of femtocells in a building results in unacceptable outage, unless intelligent interference avoidance and interference mitigation techniques are put in place.

Clearly isolation of a cell by wall penetration loss is an inherent property of indoor femtocell networks which can be utilised as a means of interference mitigation. Let Ω_j be the wall penetration loss between the CoI and the interfering BS j. The effect of Ω_j is examined in Figure 6 where Ω_j is assumed to be identical for all interfering BSs. It is shown that Ω_j has significant impact on the SINR of the femtocell. The outage probability drops to 3.7% when $\Omega_j = 10$ dB and to 0.5% when $\Omega_j = 15$ dB. This result implies that the implementation of the femtocell network is viable without complicated interference mitigation method if the wall isolation between BSs is provided.

In Figure 7, different wall losses, Ω_j, are considered. We examine the following scenarios:

(i) scenario 1: $\Omega_1 = \cdots = \Omega_6 = 0$ dB,

(ii) scenario 2: $\Omega_1 = \cdots = \Omega_5 = 0$ dB and $\Omega_6 = 15$ dB,

(iii) scenario 3: $\Omega_1 = \cdots = \Omega_6 = 15$ dB,

(iv) scenario 4: $\Omega_1 = \cdots = \Omega_5 = 15$ dB and $\Omega_6 = 0$ dB.

It is shown that scenarios 1 and 2 give similar performance. This means that the isolation from one or few BSs does not result in the performance improvement when the CoI is not protected from the majority of interfering BSs. On the contrary, a considerable difference is observed between scenarios 3 and 4. Significant degradation in the SINR is caused by one BS which is not isolated by the wall.

Similar behaviours are observed in Figure 8 where different BS transmission powers are considered. The effect of the uncoordinated power is examined by considering the following scenarios where $P_s^t = 20$ dBm:

(i) scenario 5: $P_1^t = \cdots = P_6^t = 20$ dBm,

(ii) scenario 6: $P_1^t = P_2^t = P_3^t = 30$ dBm and $P_4^t = P_5^t = P_6^t = 10$ dBm,

(iii) scenario 7: $P_1^t = P_2^t = P_3^t = 25\,\text{dBm}$ and $P_4^t = P_5^t = P_6^t = 20\,\text{dBm}$,

(iv) scenario 8: $P_1^t = 30\,\text{dBm}$ and $P_2^t = \cdots = P_6^t = 20\,\text{dBm}$.

Figure 8 shows the CDFs of SINR by FW method with the assumption that $\Omega_j = 0\,\text{dB}\ \forall j$. It is observed that scenario 6 results in the worst SINR. This means that the higher transmission powers of a few BSs result in significantly decreased SINR. However, reduced transmission power in only a subset of neighbouring BSs does not necessarily improve the SINR because the predominant interference largely depends on the BSs which use high transmission powers. A similar trend is shown when comparing scenario 7 and scenario 8. The SINR performance is worse in scenario 8 than in scenario 7 for the same reason.

Finally, the effects of the BSs transmission power and the background noise are shown in Figure 9. If the transmit power drops below a certain level, a change in the PDF can be observed. For 10 dBm transmit power, for example, a noticeable impairment of the SINR can be seen. This is because the noise power remains the same regardless of the transmission power. In the case of increased transmission power, however, little change in the SINR distribution is observed. This means that the SINR is already interference limited with a transmission power of 20 dBm. Thus, the increase in the transmit power of BSs does not result in an improvement as expected.

4. Conclusion

In this paper, the PDF of the SINR for the downlink of a cell has been derived in a semianalytical fashion. It models an uncoordinated deployment of BSs which is particularly useful for the analysis of femtocells in an indoor environment. A practical propagation model including log-normal shadow fading is considered in the derivation of the PDF. The PDF presented in this paper has been obtained through analysis and calculated through standard numerical methods. The comparison with Monte Carlo simulation shows a good agreement, which indicates that the semianalytical PDF obviates the need for complicated and time-consuming simulations. The results also provide some insights into the performance of the indoor femtocells with universal frequency reuse. First, significant outage can be expected for a scenario where femto BSs are densely deployed in an in-building environment. This highlights that interference avoidance and mitigation techniques are needed. The isolation offered by wall penetration loss is an attractive solution to cope with the interference. Second, the SINR can be worsened by uncoordinated transmission powers of BSs. Thus, a coordination of BSs transmission power is needed to prevent a significant decrease in SINR.

Acknowledgment

This work was supported by the National Research Foundation of Korea, Grant funded by the Korean Government (NRF-2007-357-D00165).

References

[1] A. J. Viterbi, A. M. Viterbi, and E. Zehavi, "Other-cell interference in cellular power-controlled CDMA," *IEEE Transactions on Communications*, vol. 42, no. 4, pp. 1501–1504, 1994.

[2] M. Zorzi, "On the analytical computation of the interference statistics with applications to the performance evaluation of mobile radio systems," *IEEE Transactions on Communications*, vol. 45, no. 1, pp. 103–109, 1997.

[3] F. Graziosi, L. Fuciarelli, and F. Santucci, "Second order statistics of the SIR for cellular mobile networks in the presence of correlated co-channel interferers," in *Proceedings of the 53th IEEE Vehicular Technology Conference (VTC '01)*, pp. 2499–2503, Rhodes, Greece, May 2001.

[4] V. Koshi, "Coverage uncertainty and reliability estimation for microcellular radio network planning," in *Proceedings of the 51th IEEE Vehicular Technology Conference (VTC '00)*, pp. 468–472, Tokyo, Japan, May 2000.

[5] D. Stachle, "An analytic method for coverage prediction in the UMTS radio network planning process," in *Proceedings of the 61th IEEE Vehicular Technology Conference (VTC '05)*, pp. 1945–1949, Stockholm, Sweden, May-June 2005.

[6] M. Pratesi, F. Santucci, F. Graziosi, and M. Ruggieri, "Outage analysis in mobile radio systems with generically correlated log-normal interferers," *IEEE Transactions on Communications*, vol. 48, no. 3, pp. 381–385, 2000.

[7] M. Pratesi, F. Santucci, and F. Graziosi, "Generalized moment matching for the linear combination of lognormal RVs: application to outage analysis in wireless systems," *IEEE Transactions on Wireless Communications*, vol. 5, no. 5, pp. 1122–1132, 2006.

[8] F. Berggren and S. B. Slimane, "A simple bound on the outage probability with lognormally distributed interferers," *IEEE Communications Letters*, vol. 8, no. 5, pp. 271–273, 2004.

[9] H. Haas and S. McLaughlin, "A derivation of the PDF of adjacent channel interference in a cellular system," *IEEE Communications Letters*, vol. 8, no. 2, pp. 102–104, 2004.

[10] A. Mudesir, M. Bode, K. W. Sung, and H. Haas, "Analytical SIR for self-organizing wireless networks," *EURASIP Journal on Wireless Communications and Networking*, vol. 2009, Article ID 912018, 8 pages, 2009.

[11] V. Chandrasekhar, J. G. Andrews, and A. Gatherer, "Femtocell networks: a survey," *IEEE Communications Magazine*, vol. 46, no. 9, pp. 59–67, 2008.

[12] Z. Bharucha and H. Haas, "Application of the TDD underlay concept to home nodeB scenario," in *Proceedings of the 7th IEEE Vehicular Technology Conference (VTC '08)*, pp. 56–60, Singapore, May 2008.

[13] Z. Bharucha, I. Ćosović, H. Haas, and G. Auer, "Throughput enhancement through femto-cell deployment," in *Proceedings of the IEEE 7th International Workshop on Multi-Carrier Systems & Solutions (MC-SS '09)*, pp. 311–319, Herrsching, Germany, May 2009.

[14] H. Claussen, "Performance of macro—and co-channel femtocells in a hierarchical cell structure," in *Proceedings of the 18th IEEE International Symposium on Personal, Indoor and Mobile Radio Communications (PIMRC '07)*, Athens, Greece, November 2007.

[15] J. Espino and J. Markendahl, "Analysis of macro—femtocell interference and implications for spectrum allocation," in *Proceedings of the 20th IEEE International Symposium on Personal, Indoor and Mobile Radio Communications (PIMRC '09)*, pp. 13–16, Tokyo, Japan, September 2009.

[16] A. Valcarce, G. D. L. Roche, A. Jüttner, D. Lopez-Perez, and J. Zhang, "Applying FDTD to the coverage prediction of wiMAX femtocells," *Eurasip Journal on Wireless Communications and Networking*, vol. 2009, Article ID 308606, 13 pages, 2009.

[17] M. Yavuz, F. Meshkati, S. Nanda, et al., "Interference management and performance analysis of UMTS/HSPA+ femtocells," *IEEE Communications Magazine*, vol. 47, no. 9, pp. 102–109, 2009.

[18] N. C. Beaulieu and Q. Xie, "An optimal lognormal approximation to lognormal sum distributions," *IEEE Transactions on Vehicular Technology*, vol. 53, no. 2, pp. 479–489, 2004.

[19] L. F. Fenton, "The sum of log-normal probability distributions in scatter transmission systems," *IRE Transactions on Communications Systems*, vol. 8, no. 1, pp. 57–67, 1960.

[20] N. B. Mehta, J. Wu, A. F. Molisch, and J. Zhang, "Approximating a sum of random variables with a lognormal," *IEEE Transactions on Wireless Communications*, vol. 6, no. 7, pp. 2690–2699, 2007.

[21] S. C. Schwartz and Y. S. Yeh, "On the distribution function and moments of power sums with log-normal components," *The Bell System Technical Journal*, vol. 61, no. 7, pp. 1441–1462, 1982.

[22] S. S. Szyszkowicz and H. Yanikomeroglu, "On the tails of the distribution of the sum of lognormals," in *Proceedings of the IEEE International Conference on Communications (ICC '07)*, pp. 5324–5329, Glasgow, UK, June 2007.

[23] H. Nie and S. Chen, "Lognormal sum approximation with type IV pearson distribution," *IEEE Communications Letters*, vol. 11, no. 10, pp. 790–792, 2007.

[24] M. Abramowitz and I. A. Stegun, "Handbook of mathematical functions with fomulas," in *Graphs, and Mathematical Tables*, Dover, New York, NY, USA, 9th edition, 1972.

[25] IST-4-027756 WINNER II, "D1.1.2 v1.2 WINNER II Channel Models," February 2008, http://www.ist-winner.org/WINNER2-Deliverables/D7.1.5_Final-Report_v1.0.pdf.

[26] T. M. Cover and J. A. Thomas, *Elements of Information Theory*, D. L. Schilling, Ed., Wiley Series in Telecommunications, John Wiley & Sons, New York, NY, USA, 1st edition, 1991.

[27] A. Persson, T. Ottosson, and G. Auer, "Inter-sector scheduling in multi-user OFDM," in *Proceedings of the IEEE International Conference on Communications (ICC '06)*, vol. 10, pp. 4415–4419, Istanbul, Turkey, June 2006.